Available online at www.sciencedirect.com

ScienceDirect

journal homepage: www.elsevier.com/locate/bbe

Original Research Article

Fully automatic ROI extraction and edge-based segmentation of radius and ulna bones from hand radiographs

Shreyas Simu [a], *Shyam Lal* [a,*], *Pranav Nagarsekar* [b], *Amrish Naik* [c]

[a] *Department of Electronics & Communication Engineering, National Institute of Technology Karnataka, Surathkal, Mangaluru, India*

[b] *Department of General Surgery, Goa Medical College, Bambolim, Goa, India*

[c] *Directorate of Health Services, Panjim, Goa, India*

ARTICLE INFO

Article history:
Received 10 March 2017
Received in revised form
20 July 2017
Accepted 30 July 2017
Available online 12 August 2017

Keywords:
Automated bone age assessment
Extraction of radius and ulna bones (RUROI)
Hand bone segmentation
Mathematical morphology
Edge-based segmentation

ABSTRACT

Bone age is a reliable measure of person's growth and maturation of skeleton. The difference between chronological age and bone age indicates presence of endocrinological problems. The automated bone age assessment system (ABAA) based on Tanner and Whitehouse method (TW3) requires monitoring the growth of radius, ulna and short bones (phalanges) of left hand. In this paper, a detailed analysis of two bones in the bone age assessment system namely, radius and ulna is presented. We propose an automatic extraction method for the region of interest (ROI) of radius and ulna bones from a left hand radiograph (RUROI). We also propose an improved edge-based segmentation technique for those bones. Quantitative and qualitative results of the proposed segmentation technique are evaluated and compared with other state-of-the-art segmentation techniques. Medical experts have also validated the qualitative results of proposed segmentation technique. Experimental results reveal that these proposed techniques provide better segmentation accuracy as compared to the other state-of-the-art segmentation techniques.

1. Introduction

UNICEF [1] survey shows that around 27 million births take place every year in India. But around 30 percent of that, which is approximately 8 million children are not registered. This is the root cause for problems like getting access to basic services and protection. According to the census report of India [2], the birth registration is less than 80 percent in 8 states (viz. Andhra Pradesh, Bihar, Chhattisgarh, Jammu and Kashmir, Jharkhand, Sikkim, Uttarakhand and Uttar Pradesh) and 2 union territories (viz. Dadra and Nagar Haveli, Lakshadweep). Birth

* *Corresponding author at*: Department of Electronics & Communication Engineering, National Institute of Technology Karnataka, Surathkal, Mangaluru 575025, India.
E-mail addresses: shreyas.ec14f09@nitk.edu.in (S. Simu), shyamfec@nitk.edu.in (S. Lal), pranav1175@yahoo.co.in (P. Nagarsekar), amrish15thmay@gmail.com (A. Naik).

http://dx.doi.org/10.1016/j.bbe.2017.07.004

registration is around 50–60 percent in other developing countries. One of the major problems and most primitive practice in India is early marriage even before the legal age of 18 years. In court cases, children without an official identity proof are susceptible to judgment as an adult rather than child or juvenile. Endocrinological problems in youngsters are evident and that is due to change in lifestyle and eating habits. Submission of fake documents for team selection of under-16 and under-19 age groups for various sports events is also prevalent in countries. Hence in order to overcome all these liabilities a fast, accurate and fully automatic age assessment system is required.

The maturity of a bone is measured by investigating the size, shape and amount of mineralization. Analyzing the degree of bone growth forms the basis for bone age assessment [3]. There are several methods available in the literature to assess bone age. One of them is the TW3 method [4] which is advantageous because it is not subjective as compared to Greulich and Pyle method (GP) [5]. The GP method is more popular due to its simplicity, as it compares a hand radiograph with few samples from an atlas organized based on the age. TW3 method is less extensively used due to its complexity, as this method analyses 13 bones (radius, ulna and short bones) of the hand to evaluate a score and eventually determine the growth through a look-up table or chart. But the modular structure of TW3 method makes it easier to automate. There are 4 major stages in the automation of BAA procedure: region of interest (ROI) extraction, segmentation of bones in the ROI, feature extraction and lastly classification based on features extracted. There have been many efforts in the direction of segmenting phalanges but very few attempts in segmenting the radius and ulna bones from hand radiograph. To develop a fairly accurate BAA system, we need to analyze all 13 bones. In this paper, we focus on extraction of the region below the carpal bones (wrist bones) called radius–ulna region of interest (RUROI) and segmentation of radius and ulna bones from that region.

Most of the work done in the field of ABAA is based on TW2 method [6] which was predecessor to TW3 method. The major difference between the two methods was that TW2 used a 20 bone score; RUS bones (radius, ulna and short bones) as well as carpal bones were used to assess the bone age. TW3 method is updated and more suitable to be used for automated bone age assessment. It uses a 13 bone score called as RUS score [4]. There have been few attempts made for extraction, pre-processing and segmentation of radius and ulna bones. Notable work was done by Pietka et al. [7,8] in extraction of Epiphysis–Metaphysis region of interest (EMROI). Chai et al. have worked on segmentation [9] and pre-processing [10] for BAA. Authors performed segmentation of the bones with a modified *k*-means algorithm. For pre-processing step they proposed a histogram equalization technique which uses multi-objective optimization technique for histogram equalization.

The two most important bones in the RUS score that were often neglected by the researchers are radius and ulna. Tristán and Arribas [11] developed an end-to-end system focussing on radius and ulna bones. It used modified *k*-means algorithm for segmentation. As a further attempt, a detailed methodology was described, but it also did not cover all the stages of TW3 [12], but in this paper accuracy and performance of the neural network was analyzed. Han et al. [13] used a coarse-to-fine strategy, where they had used two stages of segmentation. Coarse segmentation was done by using watershed transform. The finer stage involved active contour model (ACM) with gradient vector flow (GVF) snakes method. Liu et al. [14] used particle swarm optimization (PSO) in their paper for matching templates of various edges from the edge set that was created earlier. Drawback of this paper was that no result comparison was made with other techniques or using quality metrics.

Recently Guraksin et al. [15] have worked on morphological operators for pre-processing, segmentation and feature extraction. In this paper, authors have used support vector machines (SVM) for classification and their main work was focused on carpal bones and radius bone only for an age group of 0–6 years. Giordano et al. [16] designed a complete automated BAA system. In this system, the pre-processing stage involved removal of radiological markers, background removal and rotation of hand if needed. In their further work the classification was done using Hidden Markov Models (HMM) [17]. Seok et al. [18] have extracted 17 ROIs altogether from phalanges and radius, ulna bones and used multi-layered fuzzy classifiers for classification. Scale Invariant Feature Transform (SIFT) feature extraction was used for BAA by Kashif et al. [19] and later the authors proved that SIFT is better than other feature extraction techniques like BRISK, FREAK, etc. [20]. But the authors use a semiautomatic procedure involving Otsu's thresholding as the main segmentation technique.

Some state-of-the-art segmentation techniques have not been used for hand bone segmentation. One of the recent algorithm is Adaptively Regularised Kernel-based Fuzzy C-means clustering (ARKFCM) [21]. This algorithm is a modified version of fuzzy C-means algorithm. An adaptive regularization parameter is used to enhance segmentation robustness which adopts the Gaussian radial basis function (GRBF) and also makes use of weighted image for better accuracy. We have done a detailed study on evolutionary and non-evolutionary segmentation techniques on hand radiographs in our previous paper [22]. This work involved applying segmentation technique to the whole hand radiograph and not targeted to any particular region. There is still a need for improvisation in BAA system, hence RUROI extraction method and edge-based segmentation technique is proposed.

In this paper, we focus on radius and ulna bone region extraction and segmentation. The main contributions of this research paper are summarized as follows:

1. We have developed a fully automated RUROI extraction method for hand radiographs. This method is quite simple as we use simple morphological tools instead of complex mathematical steps.
2. We have proposed a fully automated segmentation technique for the segmentation of extracted ROI of radius and ulna bones. Proposed technique is based on morphological tools, active contours, level set concept and post processing.
3. Experiments have been undertaken to demonstrate the robustness of the proposed segmentation technique

in comparison to other state-of-the-art techniques from the specialized literature on publicly available image database.

This paper is organized as follows: Section 2 describes the steps followed for fully automatic ROI extraction and the edge-based segmentation technique for radius and ulna bones. In Section 3, the details of image database and the quality metrics used are described. In Section 4 we discuss the segmentation results rated by medical experts. Also in the same section a comparison between proposed segmentation technique and other state-of-the-art techniques is done with the help of quality metrics. Section 5 concludes the work.

2. Proposed fully automatic RUROI extraction and edge-based segmentation technique

This section presents detailed mathematical analysis of proposed RUROI extraction and edge-based segmentation technique. In the first phase we propose a fully automated ROI extraction of radius and ulna bones from hand radiographs. In the second phase we propose an improved edge-based segmentation technique for extracted ROI of radius and ulna bones. The block diagram of the whole procedure is given in Fig. 1, with the individual blocks described.

2.1. *Automated radius–ulna ROI (RUROI) extraction*

Morphological operators [23] are used for extraction of RUROI along with some basic mathematical operations. The RUROI extraction procedure and the steps are as follows:

1. The input hand radiograph R is subjected to Gaussian filtering for noise removal [24].
2. Multi-level Otsu thresholding to get the boundary of hand [25]. The output image of this step is referred as I.
3. Morphological erosion to smoothen the boundary of hand. The morphological erosion operation on an input image I by structuring element S is given by equation:
$$I \ominus S = x : S_x \subset I \tag{1}$$
where $\subset$ denotes subset. $I \ominus S$ is made up of all the points x for which the translation of S by x fits in I [23]. The output image of this step is J.
4. Unnecessary objects present in the binary image are removed with the help of edge-off function and area opening function. The edge-off function discards any object connected to borders of the image. Area open filter removes an object from the image if its size is less than some value ζ.
$$J \circ (\zeta)_n = \bigcup P, area(P) \geq \zeta \tag{2}$$
where J is the input image and P is the area of n-connected component [23].
5. Find the mean of all columns of the binary image. Use the column with maximum value as a reference line for finding the vertical borders of the ROI.
6. With the help of reference column from previous step which divides the hand into two parts, find the first non-zero values from the left and right borders of hand radiograph. These non-zero values form the left and right borders of RUROI.
7. To find the top horizontal border of RUROI, we find the mean values along the rows and choose a border line of RUROI based on the information extracted.
8. Use the above properties to crop a rectangular region containing the bones radius and ulna. Let the output image of this stage be X.

As mentioned above in pre-processing step, Gaussian low pass filtering was used for noise removal where filter size is kept 3×3 and the value of σ was set to 5 [24]. The hand radiographs were not resized before applying the proposed technique. Matlab functions used are *multithresh* and SDC toolbox function *mmthreshad* for this operation [23]. The binary image obtained after thresholding is further smoothened using erosion function *mmero* as given in Eq. (1) and structuring element used here was cross with size 2. Unwanted objects present in the image were removed with the help of *mmedgeoff* and *mmareaopen* functions. The borders of RUROI have been found using simple mathematical logic as explained using MATLAB functions *mean* and *find*.

2.2. *Edge-based segmentation*

The RUROI image X can be written in terms of following equation:

$$X = bY + n \tag{3}$$

where b denotes the bias field, Y stands for true image and n represents additive noise. The true image has been mixed with bias field and additive noise, which makes it difficult to extract. We modify the image in such a way that edges and other features are enhanced. This is achieved by three steps:

1. Use alternating sequential filtering to diffuse the image with less effect on the edges and curves [23]. We have used close-open filter with $m = 3$:
$$F_{CO}^{m} = (((((X \bullet S) \circ S) \bullet 2S) \circ 2S) \ldots \bullet mS) \circ mS \tag{4}$$
where m is number of times structuring element S is applied to the image X.
2. Take morphological gradient of negative image of resulting filtered image.
$$K = (\sim F \oplus S) - (\sim F \ominus S) \tag{5}$$
where $\sim F$ is compliment of image F, $\oplus$ and $\ominus$ are dilation and erosion operators respectively.

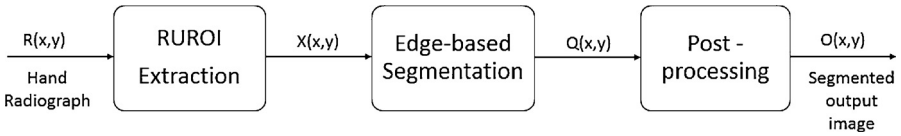

Fig. 1 – Block diagram of the proposed fully automatic RUROI extraction and segmentation of radius and ulna bones.

3. Add this image K to the original image X to get edge-enhanced image A.

The true image Y is the representation of physical features of hand. Hence it is safe to assume that Y is approximately piecewise constant. The image A is a function $A:\Omega\rightarrow R$ defined on the continuous domain Ω. We assume that the bias field is smoothly varying. The true image Y can be divided into N different regions $\Omega=\cup_{i=1}^{N}\Omega$ with each region taking a constant value $v_1, v_2, \ldots, v_N$.

Assume c as the center point of a circular area which has radius r. We can say that $V_c = x : |x-c| < r$, where c belongs to Ω. We divide this region Ω into N different regions $\Omega_{i=1}^{N}$ [26]. From modeled expression for hand radiograph, i.e. Eq. (3) and the above said formulation we can write new equation as:

$$A(x) = b(x)v_i + n(x) \quad \text{where } x \in V_c \cap \Omega \tag{6}$$

The above equation is similar to k-means clustering [27] and can be written in continuous energy equation as:

$$E = \int_{V_c} |A(x)-q_i|^2 u_i(x)\,dx \tag{7}$$

where q_i is the cluster center of the ith cluster and u_i is the membership function of region Ω_i. We can safely assume that $q_i \approx b(x)v_i$ and defined in the region V_c. The membership function will have a value 1 in this region and zero outside, hence we can write it as:

$$E(b,v) = \int_{\Omega} |A(x)-b(x)v_i|^2\,dx \tag{8}$$

Using the Chan and Vese (CV) model [28], now level set function can be used to minimize the energy function. Level Set Methods are one of the many numerical techniques designed to track the evolution of interfaces. Level set function focuses on moving boundaries by exploiting a strong link between moving interfaces and equations from computational fluid equations [29,30]. The CV model equation is given by following equation.

$$\begin{aligned} Q(\phi, v_1, v_2) \;=\; & \int_{\Omega} |A(x)-b(x)v_1|^2\; H(\phi(x))\,dx \\ & + \int_{\Omega} |A(x)-b(x)v_2|^2\; (1-H(\phi(x)))\,dx \\ & + \chi \int_{\Omega} |\nabla H(\phi(x))|\,dx \end{aligned} \tag{9}$$

where ϕ is the level set function and H is the Heaviside function. The Heaviside function is a discontinuous function which is zero for all negative arguments and one for all positive arguments. The first two terms in Eq. (9) are data fitting terms, whereas the last term regularizes the zero level contour [29]. The level set function performs division of the image into two parts $\Omega_1 = x : \phi(x) < 0$ and $\Omega_2 = x : \phi(x) > 0$. Hence the segmentation of radius and ulna bones is fulfilled by finding parameters like level set function ϕ and the constants v_1 and v_2 that minimize the energy function.

We define $u_1(\phi) = H(\phi)$ and $u_2(\phi) = 1 - H(\phi)$ to divide the image into object and background, where u_i represents membership function for the regions Ω_i. This revises the energy function and now it can be defined as:

$$E(b,v,\phi) = \int_{\Omega} \sum_{i=1}^{N} |A(x)-b(x)v_i|^2 u_i(\phi(x))\,dx \tag{10}$$

Now this energy term is used as data term in Eq. (9) and the equation is rewritten as:

$$Q(b,v,\phi) = E(b,v,\phi) + \chi W(\phi) \tag{11}$$

where χ is the weight and $W(\phi)$ is the regularization term which is equal to $\int_{\Omega} |\nabla H(\phi(x))|dx$. We minimize Eq. (11) with respect to variables b, v and ϕ to segment the bones from RUROI. The minimization is achieved by performing iterations, where in each iteration we fix any two variables and minimize Eq. (11) with respect to the third variable, the steps are:

1. Energy minimization with respect to ϕ: For fixed values of v and b the minimization of $Q(b,v,\phi)$ can be achieved by using gradient descent method.

$$\frac{\partial \phi}{\partial t} = -\frac{\partial Q}{\partial \phi} \tag{12}$$

By using calculus of variations we have:

$$\frac{\partial \phi}{\partial t} = -\delta(\phi)(q_1 - q_2) + \chi\delta(\phi) div\left(\frac{\nabla(\phi)}{|\nabla(\phi)|}\right) \tag{13}$$

where $q_i = \int |A(x)-b(x)v_i|^2\,dx$ and $i = 1, 2$.

2. Energy minimization with respect to v: For fixed values of ϕ and b, the optimized value of v can be denoted as:

$$v\prime_i = \frac{\int bA(x)u_i(\phi(x))\,dx}{\int b^2 u_i(\phi(x))\,dx} \quad \text{where } i = 1, 2 \tag{14}$$

3. Energy minimization with respect to b: For fixed values of ϕ and v, the optimized value of b can be denoted as:

$$b\prime = \frac{A(x)[(v_1 u_1(\phi(x))) + (v_2 u_1(\phi(x)))]}{[(v_1^2 u_1(\phi(x))) + (v_2^2 u_1(\phi(x)))]} \tag{15}$$

Implementation details of edge-based segmentation are described here. Function *mmasfrec* was used for alternate sequential filtering of image. Close-open-close filtering was done as value of m chosen was 3. Structuring element used was disk with size 1. Further *mmgradm* function was used to get the gradient. Structuring element used for this function was disk with size 2. Level set contour has been initialized randomly on the image as contours initialized in a shape of box or circle get trapped in some regions. Smoothed version of Heaviside function [29] is used for implementation purposes which is defined in Eq. (16):

$$H_v(x) = \frac{1}{2}\left[1 + \frac{2}{\pi}\arctan\left(\frac{x}{v}\right)\right] \tag{16}$$

where $v = 1$ as done in [28]. The value of χ, weight of regularization term in Eq. (11) is set to any smaller value or it is made equal to the standard deviation of the extracted ROI image. The number of iterations is set to 100.

2.3. *Post-processing*

The importance of this stage lies in the fact that extracting accurate information from the segmented bones will help in further stages of BAA system. The level set contours initialized to track the bone edges may not behave in the required way. This may be due to couple of reasons. Cancellous bone may get

tracked by the contour besides cortical bone. Cortical bone or compact bone comprises of the exterior part of bone where as cancellous bone is the internal bone region. Also intensity inhomogeneity and overlapping pixels between the soft tissue region and bone results in it getting identified as an object of interest. In some cases irregularities may be developed in the level set function during its evolution [26]. These errors are mitigated by using morphological operators. The post processing steps which give the final segmented output image $O(x, y)$ are as follows:

1. Image filling function along with erosion and dilation operations. The dilation of binary image Q by structuring element S is given by [23]:
$$Q \oplus S = (Q' \ominus S^*)' \quad (17)$$
The dilation of Q by S is done by rotating S around origin to get S^* and then Q' which is a complement of Q is eroded by S^*.
2. Area opening function as given in Eq. (2) along with erosion operation given in Eq. (1) and dilation operations mentioned in Eq. (17).
3. Edge off function to remove any unnecessary objects and carpal bones present at the edge of image.

The functions such as image filling function *imfill* and dialtion operation *mmdil* are used for post processing. Area-opening function *mmareaopen* and edge-off function *mmedgeoff* are used to remove carpal bones and other vestigial parts present in the ROI.

The step by step workflow of the proposed automatic RUROI extraction and segmentation technique is shown in Fig. 2.

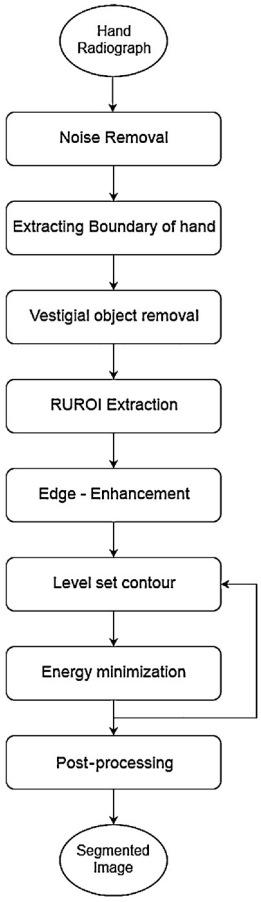

Fig. 2 – Workflow of the proposed fully automatic RUROI extraction and segmentation of radius and ulna bones.

2.4. *Illustration of the proposed technique*

The proposed technique is divided into 2 major stages as discussed earlier which are RUROI extraction and edge-based segmentation. The latter stage can be further sub-divided into edge-enhancement, segmentation and post-processing stages. Quantitative results of each stage have been evaluated using the quality metrics (QM) like peak signal-to-noise ratio (PSNR), mean square error (MSE), structure similarity index (SSIM) [22] which are given in Table 1. Please note that the edge-enhanced image is compared with RUROI image and the output image of other two stages are compared with ground truth image for calculating PSNR, MSE and SSIM. Output images of each stage is given in Figs. 3–5 respectively. After edge-enhancement stage, we have achieved clear demarkation of edges which is apparent in Figs. 3–5. Fig. 3 shows the implementation of proposed technique on hand radiograph of 1 year old child. The smaller bone is ulna and the larger is radius. The small bone above radius is called epiphysis which will fuse with metaphysis of radius as the child grows. Metaphysis is the head portion of any bone. These bones are a part of analysis for BAA [3,4]. Similarly for hand radiograph of 7 year old, the output images are presented in Fig. 4. A part of carpal bone is present in RUROI, which has been removed after post-processing. We can see in Fig. 4 the epiphsis has grown in size and will later fuse with radius bone. In Fig. 5, we have

Table 1 – Performance results after each stage of the proposed technique.

Image	QM	Edge-enhancement	Segmentation	Post-processing
1 year [5173.jpg]	PSNR	33.109	46.471	65.891
	MSE	31.781	1.466	0.017
	SSIM	0.967	0.847	0.999
7 years [5154.jpg]	PSNR	32.150	47.430	65.172
	MSE	39.635	1.175	0.020
	SSIM	0.960	0.881	0.999
18 years [6145.jpg]	PSNR	30.751	45.941	68.753
	MSE	54.702	1.656	0.009
	SSIM	0.956	0.830	0.999

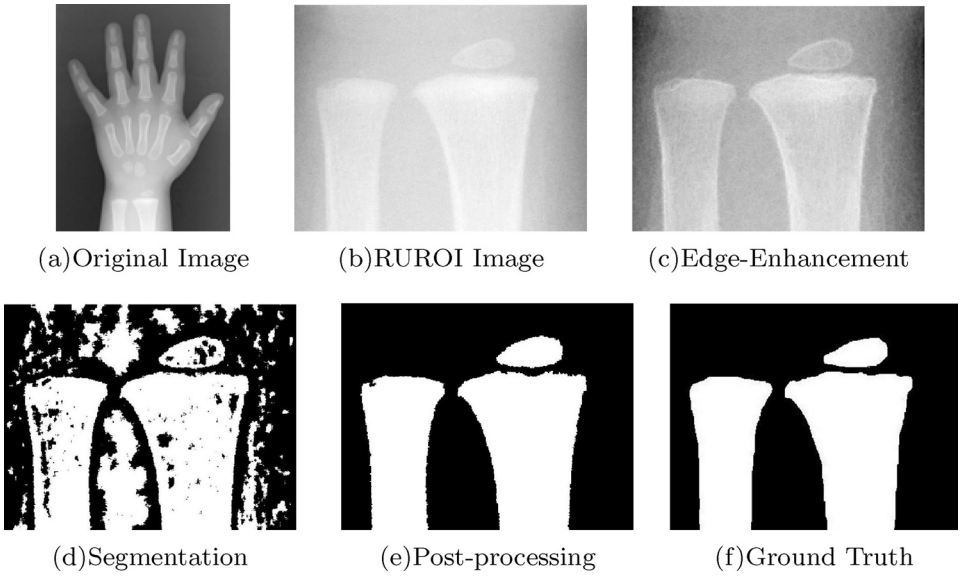

Fig. 3 – Output images from each stage of the proposed technique on hand radiograph of 1 year old [5173.jpg].

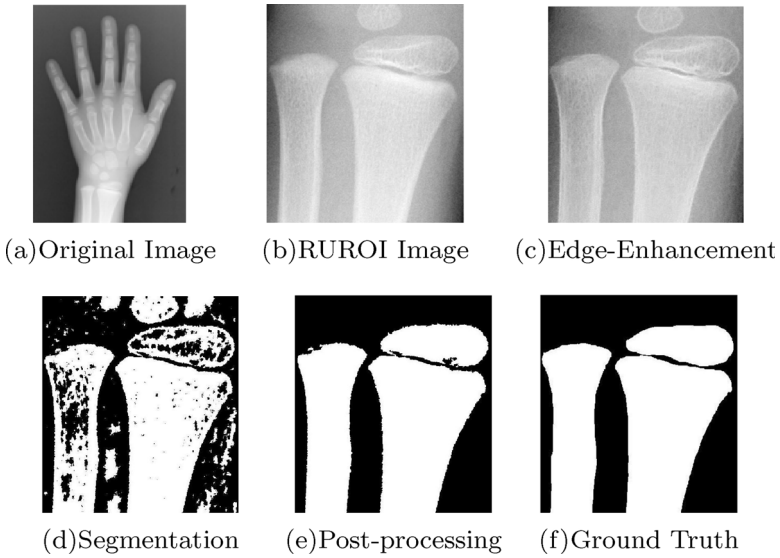

Fig. 4 – Output images from each stage of the proposed technique on hand radiograph of 7 year old [5154.jpg].

presented the output images of hand radiograph of 18 year old person at each stage of proposed technique.

3. Materials and methods

We have compared the proposed segmentation technique with popular and widely used segmentation techniques such as *k*-means clustering technique (M1) [31], adaptive clustering technique based on *k*-means and Gibb's random fields (KGRF) (M2) [32], PSO based segmentation technique (M3) [33], DPSO based segmentation technique (M4) [34], and Adaptively Regularised Kernel-based Fuzzy C-means clustering (ARKFCM) technique (M5) [21]. These techniques have been implemented on digital hand radiographs within an age group of 0–18 years. Table 2 shows the parameters used for these segmentation techniques and their values. The first three techniques namely M1, M2 and M3 have been used in the field of hand bone segmentation earlier [8,11,14]. DPSO is a popular optimization technique which has been explored in this paper. ARKFCM is a recent algorithm which has also been included for comparison. More details about the techniques used for comparison can be obtained from the respective papers mentioned above.

Specifications of the system from which results were obtained are: Intel i7 processor with clock speed of 3.6 GHz and 8 GB RAM. MATLAB 2015a was used for implementing the RUROI extraction and all the segmentation techniques.

3.1. *Image database*

The database of digital hand radiographs [35] is freely available for research purposes on an online website, http://www.ipilab.org/BAAweb/. We have downloaded the database from this website in which the images were collected from Children's

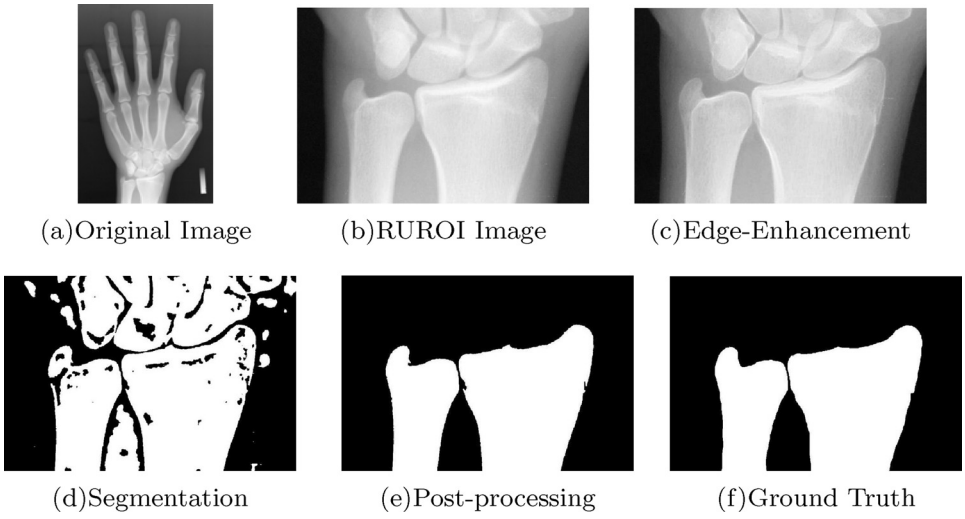

Fig. 5 – Output images from each stage of the proposed technique on hand radiograph of 18 year old [6145.jpg].

Table 2 – Parameters used for compared segmentation techniques and their values.

Parameters	M1	M2	M3	M4	M5	PT
Number of clusters	3	3	3	3	3	
Number of iterations		30	150	150		100
Clique potential		0.5				
Local filtering					Median	Gaussian
Local window size					3	3
Population			150	30		
Inertial weight			1.2	1.2		
Weight 1			0.8	0.8		
Weight 2			0.8	0.8		
Min velocity			−5	−1.5		
Max velocity			5	1.5		
Lower bound of position			1	1		
Upper bound of position			256	256		
Stagnancy				10		
Time step						0.1
Heaviside weight						1

Hospital Los Angeles, USA. This database contains 1371 hand radiograph images which can be further divided into 696 images of males and 675 images of females. This database is also categorized based on races, Asian, Black, Caucasian and Hispanic. It contains hand radiographs of infants to that of 18 years old person. We also prepared a database of ground truth images with the help of medical experts from Goa Medical College (GMC), Bambolim, Goa, India and used it for result comparison.

3.2. *Quality metrics*

We have presented implementation results acquired from 50 images in Section 4. Performance evaluation of segmentation result is done using standard quality metrics like SSIM, Jaccard Similarity Index (JSI), Dice, Accuracy, Geometric Mean (GM) and Matthews Correlation Coefficient (MCC). [22,36]

4. Results and discussion

This section presents experimental results of RUROI extraction and different segmentation techniques including proposed technique on digital hand radiographs. In the simulation, 50 hand radiographs have been considered for experimentation [35]. The results of 19 images, one for each age, have been presented in the following subsection.

4.1. *RUROI extraction results*

RUROI is extracted according to the recommendations given in literature [4]. To calculate the RUS score we need radius and ulna bones along with its epiphyseal plate. RUROI images extracted from the digital hand radiographs are shown in Fig. 6. Some of the carpal bones (wrist bones) will be present in the RUROI owing to the close proximity of these bones toward radius and ulna bones. The sizes of RUROI's will be different for each image owing to fact that the extraction technique fits around radius and ulna bones region.

4.2. *Performance evaluation*

The performance comparison using different quality metrics are presented in Tables 3 and 4 and they provide valuable information about the quality of segmentation performed. The quantitative results comparison between various

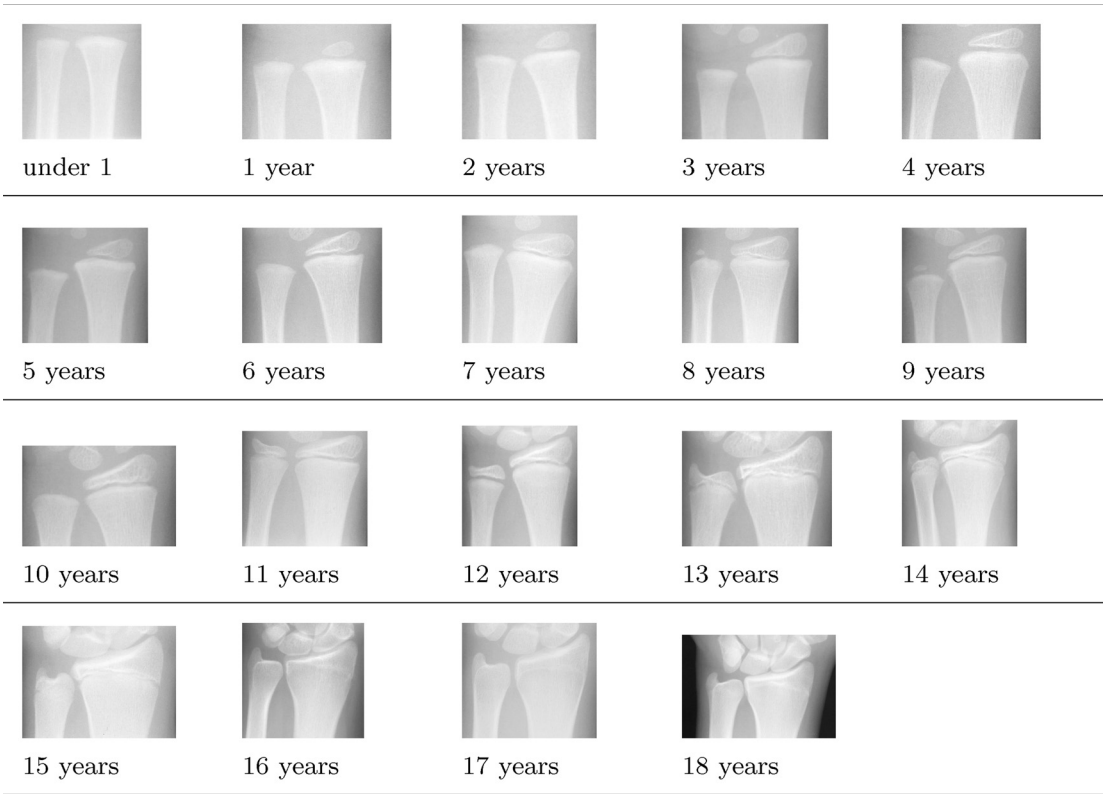

Fig. 6 – RUROI images extracted from digital hand radiographs.

Table 3 – Performance comparison between different segmentation techniques on RUROI based of various quality metrics.

Image	QM	M1	M2	M3	M4	M5	PT
Under 1 year [5605.jpg]	SSIM	0.965	0.984	0.985	0.985	0.984	**0.996**
	JSI	0.596	0.716	0.706	0.706	0.703	**0.941**
	DICE	0.747	0.834	0.828	0.828	0.826	**0.970**
	ACC	0.798	0.858	0.853	0.853	0.852	**0.971**
	GM	0.837	0.855	0.853	0.853	0.846	**0.971**
	MCC	0.638	0.710	0.701	0.701	0.697	**0.942**
1 year [5173.jpg]	SSIM	0.980	0.981	0.981	0.983	0.965	**0.999**
	JSI	0.688	0.695	0.685	0.695	0.570	**0.956**
	DICE	0.815	0.820	0.813	0.820	0.726	**0.977**
	ACC	0.844	0.847	0.843	0.848	0.785	**0.978**
	GM	0.827	0.865	0.862	0.864	0.782	**0.978**
	MCC	0.610	0.711	0.704	0.710	0.472	**0.956**
2 years [5234.jpg]	SSIM	0.967	0.980	0.980	0.981	0.985	**0.998**
	JSI	0.629	0.702	0.702	0.704	0.717	**0.948**
	DICE	0.772	0.825	0.825	0.826	0.835	**0.973**
	ACC	0.814	0.851	0.851	0.852	0.858	**0.974**
	GM	0.848	0.858	0.861	0.860	0.850	**0.974**
	MCC	0.667	0.704	0.707	0.706	0.717	**0.948**
3 years [6102.jpg]	SSIM	0.986	0.986	0.986	0.987	0.960	**0.999**
	JSI	0.728	0.745	0.742	0.744	0.570	**0.960**
	DICE	0.843	0.854	0.852	0.853	0.726	**0.980**
	ACC	0.864	0.872	0.871	0.872	0.785	**0.980**
	GM	0.832	0.867	0.871	0.871	0.862	**0.984**
	MCC	0.623	0.743	0.738	0.738	0.740	**0.969**
4 years [5095.jpg]	SSIM	00.986	0.984	0.986	0.986	0.965	**0.998**
	JSI	0.753	0.709	0.732	0.732	0.628	**0.948**
	DICE	0.859	0.829	0.845	0.845	0.772	**0.973**
	ACC	0.877	0.854	0.866	0.866	0.814	**0.974**
	GM	0.868	0.842	0.856	0.856	0.851	**0.975**
	MCC	0.766	0.731	0.746	0.746	0.671	**0.949**

Table 3 (*Continued*)

Image	QM	M1	M2	M3	M4	M5	PT
5 years [7143.jpg]	SSIM	0.988	0.987	0.988	0.987	0.983	**0.998**
	JSI	0.754	0.747	0.755	0.739	0.677	**0.950**
	DICE	0.860	0.855	0.861	0.850	0.808	**0.974**
	ACC	0.877	0.873	0.878	0.870	0.839	**0.975**
	GM	0.879	0.864	0.870	0.860	0.823	**0.981**
	MCC	0.766	0.760	0.764	0.753	0.708	**0.963**
6 years [5134.jpg]	SSIM	0.981	0.989	0.989	0.990	0.989	**0.989**
	JSI	0.717	0.773	0.770	0.771	0.765	**0.765**
	DICE	0.835	0.872	0.870	0.870	0.867	**0.867**
	ACC	0.859	0.887	0.885	0.885	0.883	**0.883**
	GM	0.872	0.883	0.883	0.882	0.876	**0.876**
	MCC	0.728	0.771	0.767	0.768	0.768	**0.768**
7 years [5154.jpg]	SSIM	0.982	0.980	0.982	0.982	0.978	**0.999**
	JSI	0.735	0.715	0.723	0.715	0.677	**0.964**
	DICE	0.847	0.834	0.839	0.834	0.808	**0.982**
	ACC	0.868	0.858	0.861	0.857	0.839	**0.982**
	GM	0.854	0.847	0.853	0.853	0.835	**0.979**
	MCC	0.681	0.721	0.724	0.724	0.707	**0.959**
8 years [5054.jpg]	SSIM	0.984	0.982	0.985	0.985	0.981	**0.998**
	JSI	0.726	0.688	0.720	0.721	0.663	**0.943**
	DICE	0.841	0.815	0.837	0.838	0.798	**0.971**
	ACC	0.863	0.844	0.860	0.861	0.832	**0.972**
	GM	0.854	0.830	0.854	0.853	0.815	**0.972**
	MCC	0.731	0.708	0.716	0.720	0.691	**0.943**
9 years [7161.jpg]	SSIM	0.983	0.982	0.983	0.983	0.983	**0.998**
	JSI	0.707	0.710	0.714	0.714	0.687	**0.945**
	DICE	0.828	0.830	0.833	0.833	0.815	**0.972**
	ACC	0.853	0.855	0.857	0.857	0.844	**0.972**
	GM	0.845	0.850	0.855	0.853	0.831	**0.972**
	MCC	0.704	0.704	0.708	0.709	0.697	**0.945**

The bold values indicate the best result obtained among all.

Table 4 – Performance comparison between different segmentation techniques on RUROI based of various quality metrics.

Image	QM	M1	M2	M3	M4	M5	PT
10 years [7076.jpg]	SSIM	0.976	0.983	0.983	0.983	0.971	**0.999**
	JSI	0.673	0.723	0.718	0.718	0.644	**0.963**
	DICE	0.805	0.839	0.836	0.836	0.784	**0.981**
	ACC	0.837	0.861	0.859	0.859	0.822	**0.981**
	GM	0.850	0.862	0.863	0.862	0.834	**0.980**
	MCC	0.675	0.719	0.717	0.717	0.684	**0.962**
11 years [5506.jpg]	SSIM	0.976	0.971	0.974	0.973	0.970	**0.998**
	JSI	0.712	0.614	0.641	0.629	0.592	**0.960**
	DICE	0.832	0.760	0.781	0.772	0.744	**0.979**
	ACC	0.856	0.807	0.820	0.814	0.796	**0.980**
	GM	0.855	0.785	0.803	0.795	0.771	**0.980**
	MCC	0.706	0.624	0.645	0.637	0.615	**0.960**
12 years [5322.jpg]	SSIM	0.974	0.969	0.973	0.972	0.970	**0.998**
	JSI	0.648	0.580	0.620	0.607	0.589	**0.942**
	DICE	0.786	0.734	0.765	0.756	0.741	**0.970**
	ACC	0.824	0.790	0.810	0.804	0.795	**0.971**
	GM	0.780	0.775	0.802	0.794	0.791	**0.969**
	MCC	0.571	0.562	0.606	0.592	0.587	**0.941**
13 years [5213.jpg]	SSIM	0.976	0.973	0.974	0.974	0.973	**0.997**
	JSI	0.707	0.669	0.686	0.686	0.668	**0.950**
	DICE	0.828	0.802	0.814	0.814	0.801	**0.974**
	ACC	0.853	0.834	0.843	0.843	0.834	**0.975**
	GM	0.851	0.827	0.837	0.837	0.826	**0.975**
	MCC	0.700	0.660	0.678	0.678	0.659	**0.950**

Table 4 (*Continued*)

Image	QM	M1	M2	M3	M4	M5	PT
14 years [5237.jpg]	SSIM	0.968	0.968	0.970	0.970	0.963	**0.997**
	JSI	0.568	0.563	0.594	0.585	0.616	**0.930**
	DICE	0.724	0.721	0.745	0.738	0.762	**0.964**
	ACC	0.784	0.782	0.797	0.793	0.808	**0.965**
	GM	0.802	0.761	0.784	0.784	0.759	**0.954**
	MCC	0.603	0.547	0.577	0.577	0.546	**0.914**
15 years [4340.jpg]	SSIM	0.973	0.971	0.975	0.974	0.971	**0.998**
	JSI	0.682	0.655	0.693	0.689	0.645	**0.957**
	DICE	0.811	0.791	0.819	0.816	0.784	**0.978**
	ACC	0.841	0.827	0.847	0.844	0.822	**0.978**
	GM	0.845	0.827	0.854	0.850	0.820	**0.978**
	MCC	0.679	0.646	0.694	0.688	0.634	**0.957**
16 years [5257.jpg]	SSIM	0.964	0.963	0.964	0.964	0.963	**0.998**
	JSI	0.570	0.550	0.557	0.551	0.535	**0.958**
	DICE	0.726	0.710	0.716	0.710	0.697	**0.978**
	ACC	0.785	0.775	0.779	0.775	0.767	**0.979**
	GM	0.781	0.756	0.762	0.762	0.758	**0.959**
	MCC	0.562	0.528	0.535	0.535	0.530	**0.922**
17 years [5920.jpg]	SSIM	0.970	0.970	0.973	0.972	0.970	**0.998**
	JSI	0.669	0.635	0.657	0.646	0.622	**0.964**
	DICE	0.801	0.776	0.793	0.785	0.767	**0.982**
	ACC	0.834	0.817	0.828	0.823	0.811	**0.982**
	GM	0.852	0.812	0.828	0.820	0.803	**0.982**
	MCC	0.683	0.622	0.648	0.635	0.608	**0.964**
18 years [6145.jpg]	SSIM	0.963	0.965	0.963	0.963	0.964	**0.999**
	JSI	0.544	0.546	0.543	0.543	0.546	**0.976**
	DICE	0.704	0.707	0.704	0.704	0.706	**0.988**
	ACC	0.772	0.773	0.771	0.772	0.773	**0.988**
	GM	0.815	0.811	0.817	0.817	0.815	**0.983**
	MCC	0.587	0.581	0.591	0.590	0.587	**0.966**

The bold values indicate the best result obtained among all.

segmentation techniques is given in Tables 3 and 4. Box-plot has been used to compare all the segmentation techniques with respect to various quality metrics and has been shown in Fig. 7 wherein the sample size is 50 (number of images). The box in box-plot denotes interquartile range (IQR) and whiskers which are denoted by line with breaks define the range. Median is denoted by a line in the IQR and the crosshair mark indicates outliers. Table 5 shows the statistical values

Table 5 – Statistical values of various quality metrics against segmentation techniques.

QM	Statistic	M1	M2	M3	M4	M5	PT
SSIM	MIN	0.956	0.953	0.959	0.959	0.954	0.996
	MAX	0.989	0.992	0.992	0.993	0.995	0.999
	MEAN	0.976	0.977	0.979	0.979	0.975	0.998
	MEDIAN	0.976	0.979	0.980	0.981	0.974	0.998
	SDEV	0.008	0.008	0.008	0.008	0.009	0.001
JSI	MIN	0.537	0.477	0.537	0.537	0.473	0.903
	MAX	0.806	0.804	0.795	0.797	0.849	0.976
	MEAN	0.672	0.669	0.680	0.677	0.642	0.945
	MEDIAN	0.679	0.678	0.693	0.688	0.640	0.947
	SDEV	0.065	0.069	0.061	0.062	0.073	0.013
DICE	MIN	0.699	0.646	0.699	0.699	0.642	0.949
	MAX	0.892	0.891	0.886	0.887	0.918	0.988
	MEAN	0.802	0.800	0.808	0.806	0.780	0.972
	MEDIAN	0.809	0.808	0.819	0.815	0.781	0.973
	SDEV	0.047	0.051	0.044	0.045	0.054	0.007
ACC	MIN	0.769	0.739	0.769	0.769	0.736	0.951
	MAX	0.903	0.902	0.897	0.899	0.925	0.988
	MEAN	0.836	0.834	0.840	0.838	0.821	0.973
	MEDIAN	0.839	0.839	0.847	0.844	0.820	0.973
	SDEV	0.032	0.034	0.031	0.031	0.037	0.006

Table 5 (*Continued*)

QM	Statistic	M1	M2	M3	M4	M5	PT
GM	MIN	0.766	0.704	0.750	0.750	0.700	0.954
	MAX	0.899	0.904	0.898	0.899	0.922	0.984
	MEAN	0.837	0.829	0.838	0.836	0.816	0.972
	MEDIAN	0.839	0.837	0.847	0.844	0.822	0.973
	SDEV	0.030	0.039	0.033	0.033	0.041	0.007
MCC	MIN	0.552	0.447	0.511	0.511	0.442	0.906
	MAX	0.806	0.804	0.793	0.795	0.850	0.969
	MEAN	0.672	0.668	0.677	0.675	0.649	0.945
	MEDIAN	0.680	0.683	0.691	0.684	0.659	0.945
	SDEV	0.062	0.075	0.065	0.066	0.081	0.013

such as minimum (MIN), maximum (MAX), mean, median and standard deviation (SDEV) of various quality metrics against segmentation techniques.

The qualitative results of proposed segmentation technique (PT) and other state-of-the-art techniques are given in Figs. 8 and 9 for ages 0–18 years old respectively. The ground truth images have also been shown in the figures.

4.3. *Segmentation accuracy*

The ratings given by different medical experts for the results of proposed segmentation technique are mentioned in Table 6. Medical experts who analyzed the results are physicians, orthopedicians and pediatricians. These ratings used for denoting segmentation accuracy of proposed technique are

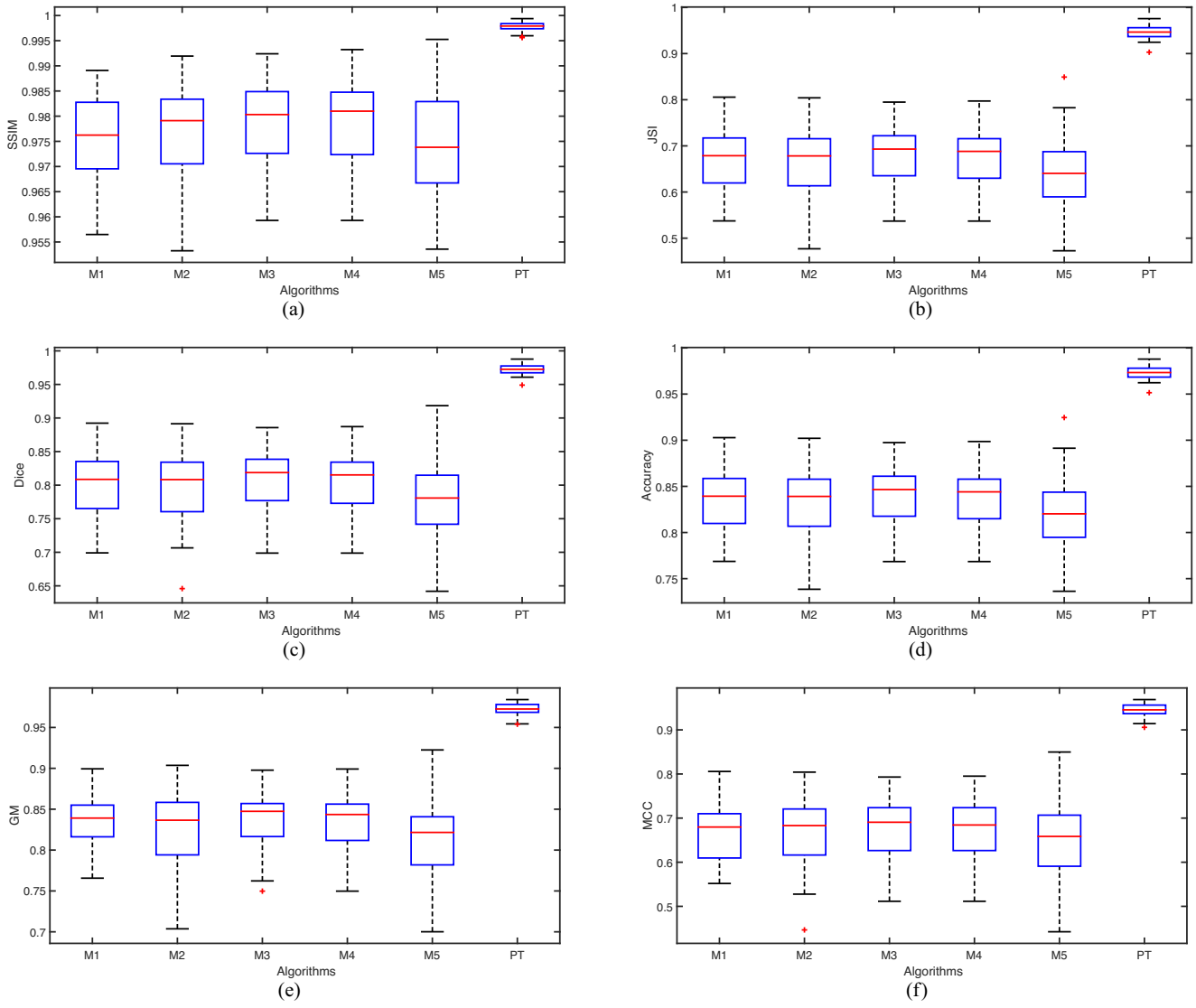

Fig. 7 – Boxplots of segmentation techniques against various quality metrics.

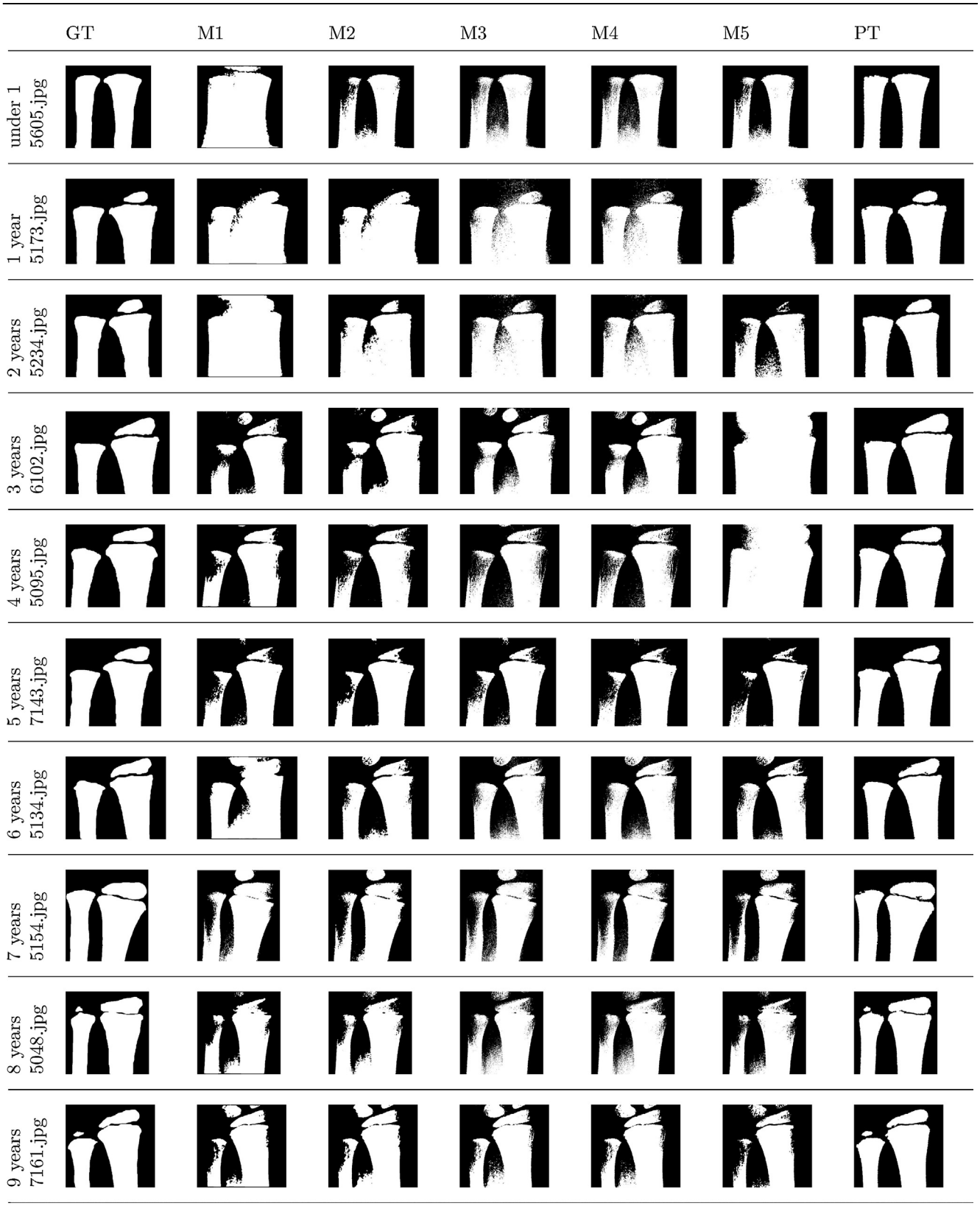

Fig. 8 – Segmentation results of different techniques on RUROI of different ages.

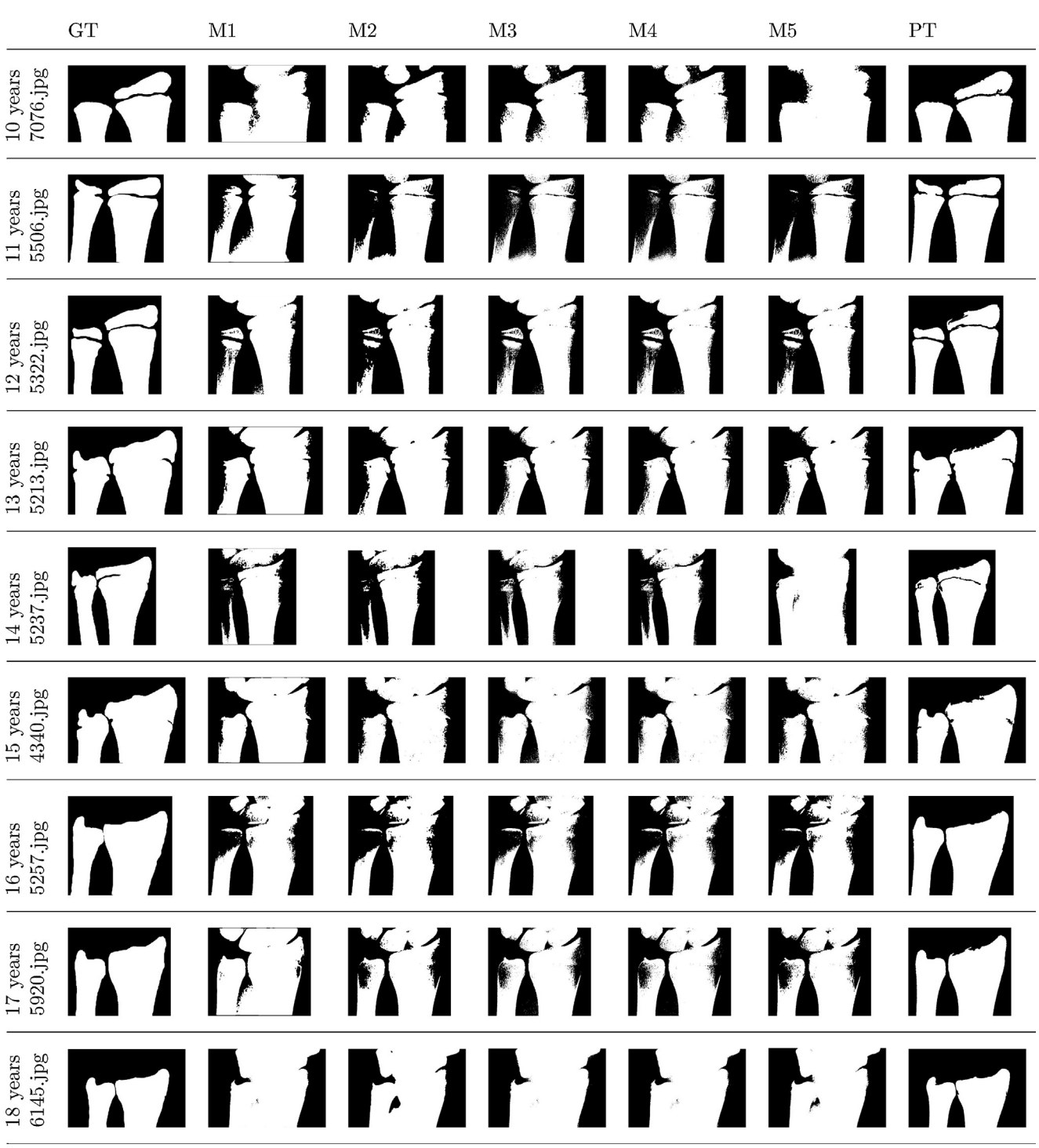

Fig. 9 – Segmentation results of different techniques on RUROI of different ages.

given after assessment by same medical experts who created the ground truth images for hand radiographs. The ratings are given between values 1–5 with value 1 being very poor, it means that segmentation technique has completely failed to delineate bones. If the value awarded is 2, it means that the bones are delineated but not completely. The value 3 is for an average result wherein bones are delineated but some blemishes still persist. If the result is good value 4 gets awarded and 5 is given when excellent result achieved, where there is seemingly no difference between the ground truth and result obtained. In Table 6, average value of ratings is calculated for each year given by a particular expert and then overall average of 4 experts is mentioned in final column.

4.4. *Discussion*

From Section 4.2, it is clear that SSIM, JSI, Dice, Accuracy, GM and MCC provide indispensable information regarding

Table 6 – Ratings given by medical experts to the segmentation results of RUROI for our proposed technique.

Age (years)	Expert-1	Expert-2	Expert-3	Expert-4	Overall average
0	4	4	4	4	4
1	4	5	5	5	4.75
2	5	5	5	5	5
3	5	5	5	5	5
4	4	4.5	4.5	4	4.25
5	4	4	4	4	4
6	4	5	5	5	4.75
7	5	5	5	5	5
8	3	3.5	3.5	4	3.5
9	5	5	5	5	5
10	4	4.5	4.5	4	4.25
12	4	4	4.5	4.5	4.25
13	4.5	4.5	5	5	4.75
14	4	4	4.5	4.5	4.25
15	5	5	5	5	5
16	4.5	5	5	4.5	4.75
17	5	5	5	5	5
18	5	5	5	5	5

the precision of segmented output from the various segmentation techniques used for comparison. From the box-plot in Fig. 7 we can clearly see that proposed segmentation technique (PT) has very less variation as compared to other techniques. It also achieves a higher segmentation accuracy among all the techniques compared, with respect to all quality metric values. SSIM values of all techniques are above 0.95 but proposed technique has value of almost 1 as shown in Fig. 7(a). The box-plot of JSI shows that *k*-means, KGRF, PSO and DPSO have similar ranges shown in Fig. 7(b), also the proposed technique takes the value around 0.9. The box-plot of Dice is similar to that one of JSI shown in Fig. 7(c), the value obtained by PT is more than 0.95 and super-seeds other state-of-the-art techniques. Similarly in other box-plots i.e. Fig. 7(d), (e) and (f) PT has higher quality metric values ACC, GM and MCC respectively approximately around 0.95. From the segmented image results of proposed segmentation technique we can see that bones are clearly delineated and it has outperformed other state-of-the-art segmentation techniques. Figs. 8 and 9 along with the segmentation results in Tables 3 and 4 clearly show that the proposed technique gives best results among all other state-of-the-art techniques. The mean and standard deviation statistics of various quality metrics tabulated in Table 5 using the results obtained from 50 images, indicate that performance of proposed technique is best among compared segmentation techniques. The ratings given by medical experts presented in Table 6 are high, except for results of 8 year old hand radiographs, which is slightly less as the radiographs had high intensity inhomogeneity. But the ratings further strengthen the claim that proposed technique has given very good segmentation results.

5. Conclusion

The proposed technique and other existing segmentation techniques have been implemented and tested successfully on the publicly available database of an age group between 0-18 years. The techniques were implemented on a wide range of radiographs which included under-exposed as well as over-exposed images. An approximate segmentation accuracy of 98 percent is achieved by the proposed technique. The average values of various quality metrics used like SSIM, JSI, Dice, ACC, GM and MCC are 0.998, 0.945, 0.972, 0.973, 0.972 and 0.945 respectively. It is also worth mentioning that the automated RUROI extraction stage is completely independent of hand placement.

The segmentation results of proposed technique have been validated by various medical experts of the field. Mean of ratings given by all the medical experts for segmentation results are above the average value i.e. 3.5. Experimental results indicated that the proposed segmentation technique provides better results as compared to other existing state-of-the-art techniques. Prime advantage of proposed technique is effectiveness and robust nature as it can be applied to over as well as under-exposed images. We can still further improve the accuracy and also study its application to carpal bones. Nevertheless the proposed techniques can be successfully applied to hand radiographs and along with results from phalangeal segmentation we can successfully determine the age of a person. The work presented in this paper is among one of the very few papers in the domain of radius and ulna bones segmentation.

The impact of this work will be visible in birth registration, judgment of juvenile court cases and under-16, under-19 sports events. The future work in the procedure of automated bone age assessment is extraction of features and classification of the same. The number of features extracted and its importance in estimating the age plays a major role in the ABAA procedure. After completion of the whole work it will give an accurate estimation of age.

Acknowledgements

The authors would like to thank the editor and anonymous reviewers for their valuable suggestions and constructive comments which helped to improve the quality of the research paper. The authors are also grateful to Dr. Kunal Fadte from

Goa Medical College, Goa, India, for his immense help in creation of database of ground truth images. They also thank Dr. Ateeque Harlapur from Belgaum Institute of Medical Sciences, Belgaum, Karnataka, India along with Dr. Kunal Fadte for validating the segmentation results. Special thanks to the team at SDC information systems for software SDC morphology toolbox developed by them also IPILAB, USC, Los Angeles for the image database without which this would not have been possible.

REFERENCES

[1] UNICEF. The situation of children in India: a profile. New Delhi: United Nations Children's Fund/India; 2011.
[2] Census Report of India. New Delhi: Registrar General and Census Commissioner of India; 2011, http://censusindia.gov.in/.
[3] Gilsanz V, Ratib O. Hand bone age: a digital atlas of skeletal maturity. Springer Science & Business Media; 2005.
[4] Tanner J, Healy M, Goldstein H, Cameron N. Assessment of skeletal maturity and prediction of adult height: TW3 method. Saunders; 2001.
[5] Greulich WW, Pyle SI. Radiographic atlas of skeletal development of the hand and wrist. Am J Med Sci 1959;238:393.
[6] Tanner JM, Whitehouse R, Marshall W, Healty M, Goldstein H. Assessment of skeleton maturity and maturity and prediction of adult height (TW2 method); 1975.
[7] Pietka E, Gertych A, Pospiech S, Cao F, Huang H, Gilsanz V. Computer-assisted bone age assessment: image preprocessing and epiphyseal/metaphyseal ROI extraction. IEEE Trans Med Imaging 2001;20:715–29.
[8] Pietka E, Pospiech-Kurkowska S, Gertych A, Cao F. Integration of computer assisted bone age assessment with clinical PACS. Comput Med Imaging Graph 2003;27:217–28.
[9] Chai HY, Wee LK, Swee TT, Hussain S. GLCM based adaptive crossed reconstructed (ACR) k-mean clustering hand bone segmentation; 2011;192–7.
[10] Chai HY, Swee TT, Seng GH, Wee LK. Multipurpose contrast enhancement on epiphyseal plates and ossification centers for bone age assessment. Biomed Eng Online 2013;12:1–19.
[11] Tristán A, Arribas JI. A radius and ulna skeletal age assessment system. IEEE Workshop on Machine Learning for Signal Processing. IEEE; 2005. p. 221–6.
[12] Tristan-Vega A, Arribas JI. A radius and ulna TW3 bone age assessment system. IEEE Trans Biomed Eng 2008;55:1463–76.
[13] Han CC, Lee CH, Peng WL. Hand radiograph image segmentation using a coarse-to-fine strategy. Pattern Recognit 2007;40:2994–3004.
[14] Liu Z, Chen J, Liu J, Yang L. Automatic bone age assessment based on PSO. 2007 1st International Conference on Bioinformatics and Biomedical Engineering; 2007.
[15] Güraksin GE, Uğuz H, Baykan ÖK. Bone age determination in young children (newborn to 6 years old) using support vector machines. Turk J Electr Eng Comput Sci 2016;24:1693–708.
[16] Giordano D, Spampinato C, Scarciofalo G, Leonardi R. An automatic system for skeletal bone age measurement by robust processing of carpal and epiphysial/metaphysial bones. IEEE Trans Instrum Meas 2010;59:2539–53.
[17] Giordano D, Kavasidis I, Spampinato C. Modeling skeletal bone development with hidden Markov models. Comput Methods Programs Biomed 2016;124:138–47.
[18] Seok J, Kasa-Vubu J, DiPietro M, Girard A. Expert system for automated bone age determination. Expert Syst Appl 2016;50:75–88.
[19] Kashif M, Jonas S, Haak D, Deserno TM. Bone age assessment meets SIFT. SPIE Medical Imaging. International Society for Optics and Photonics; 2015. p. 941439.
[20] Kashif M, Deserno TM, Haak D, Jonas S. Feature description with SIFT, SURF, BRIEF, BRISK, or FREAK? A general question answered for bone age assessment. Comput Biol Med 2016;68:67–75.
[21] Elazab A, Wang C, Jia F, Wu J, Li G, Hu Q. Segmentation of brain tissues from magnetic resonance images using adaptively regularized kernel-based fuzzy-means clustering. Comput Math Methods Med 2015;2015.
[22] Simu S, Lal S. A study about evolutionary and non-evolutionary segmentation techniques on hand radiographs for bone age assessment. Biomed Signal Process Control 2017;33:220–35.
[23] Dougherty ER, Lotufo RA, T. I. S. for Optical Engineering SPIE for Optical Engineering. Hands-on morphological image processing, vol. 71. Washington: SPIE Optical Engineering Press; 2003.
[24] Gonzalez W, Woods RE. Eddins, digital image processing using Matlab. Third New Jersey: Prentice Hall; 2004.
[25] Otsu N. A threshold selection method from gray-level histograms. Automatica 1975;11:23–7.
[26] Li C, Huang R, Ding Z, Gatenby JC, Metaxas DN, Gore JC. A level set method for image segmentation in the presence of intensity inhomogeneities with application to MRI. IEEE Trans Image Process 2011;20:2007–16.
[27] Theodoridis S, Pikrakis A, Koutroumbas K, Cavouras D. Introduction to pattern recognition: a Matlab approach. Academic Press; 2010.
[28] Chan TF, Vese LA. Active contours without edges. IEEE Trans Image Process 2001;10:266–77.
[29] Osher S, Sethian JA. Fronts propagating with curvature-dependent speed: algorithms based on Hamilton–Jacobi formulations. J Comput Phys 1988;79:12–49.
[30] Sethian JA. Numerical methods for propagating fronts. Variational methods for free surface interfaces. Springer; 1987. p. 155–64.
[31] Hartigan JA, Wong MA. Algorithm as 136: a k-means clustering algorithm. J R Stat Soc Ser C: Appl Stat 1979;28:100–8.
[32] Pappas TN. An adaptive clustering algorithm for image segmentation. IEEE Trans Signal Process 1992;40:901–14.
[33] Eberhart C, Kennedy J, et al. A new optimizer using particle swarm theory. Proceedings of the Sixth International Symposium on Micro Machine and Human Science; 1995. p. 39–43. http://dx.doi.org/10.1109/MHS.1995.494215
[34] Tillett J, Rao T, Sahin F, Rao R. Darwinian particle swarm optimization; 2005.
[35] Gertych A, Zhang A, Sayre J, Pospiech-Kurkowska S, Huang H. Bone age assessment of children using a digital hand atlas. Comput Med Imaging Graph 2007;31:322–31.
[36] Orlando JI, Prokofyeva E, Blaschko MB. A discriminatively trained fully connected conditional random field model for blood vessel segmentation in fundus images. IEEE Trans Biomed Eng 2017;64:16–27.